Applied Thermal Engineering 246 (2024) 122915

Contents lists available at ScienceDirect

Applied Thermal Engineering

journal homepage: www.elsevier.com/locate/ate

Research Paper

Radiation-driven thermoacoustic energy conversion in absorbing media

Nathan Blanc, Guy Z. Ramon *

Department of Civil & Environmental Engineering and the Grand Technion Energy Program (GTEP), Technion - Israel Institute of Technology, Haifa, 32000, Israel

ARTICLE INFO

Keywords:
Thermoacoustics
Thermoacoustic engines
Solar energy

ABSTRACT

Thermoacoustic engines rely on an instability that can convert heat into an intense acoustic wave — oscillating pressure and velocity. Being heat-driven, thermoacoustic engines are a promising technology for solar energy conversion, potentially cheap, reliable, and robust, with no moving parts and no exotic materials. Herein, we present an as-yet overlooked mode of triggering a thermoacoustic instability in such engines, driven by radiation. This mode of operation can potentially eliminate much of the viscous losses associated with high-amplitude thermoacoustic energy conversion by eliminating the need for a solid, porous medium with which to mediate heat transfer. A theoretical framework is developed for modeling such devices, with a simplified analysis illustrating that any non-uniform, temperature-dependent heat source has the potential to trigger the thermoacoustic instability. It is then further demonstrated that radiation can indeed drive such instability, with numerical results showing that energy conversion is more substantial when the oscillation period is matched with the characteristic radiative heating time of the gas. A limit-cycle analysis indicates that, for a traveling wave acoustic field, potential efficiencies of up to 90% of Carnot's efficiency may be achieved, with power densities of up to 5 MW/m^3. While several of the assumptions made in the model likely result in lower performance for a real system, the analysis demonstrates the great potential offered by this approach, for future development.

1. Introduction

The term thermoacoustics refers, in general, to thermal interactions in sound waves. A particular form of thermoacoustic interaction occurs when a fluid is in contact with a solid media, over which a temperature gradient is imposed, large enough to trigger an acoustic instability, resulting in the spontaneous generation of intense sound waves. The instability is facilitated by appropriate phasing of heat transfer and pressure variations in the fluid. Essentially, if the gas is heated when compressed and cooled when expanded, any acoustic disturbance will be amplified, in complete analogy with the thermodynamic cycle of a heat engine. This mechanism allows for the conversion of heat to acoustic power, a form of mechanical power, which can then be used for electricity generation, cooling, and additional applications [1–5]. Thermoacoustic engines have been considered where heat is supplied by combustion [6], industrial waste [7,8] as well as solar collectors [9–11], and offer the advantage of cheap manufacturing, reliability, and high energy density [12,13].Early research on thermoacoustics was documented by Sondhaus [14], Rijke [15], and more systematically by Rott [16], demonstrating the generation of sound via heating. Using a simplified linear model, Rott demonstrated that thermoacoustic power generation (or attenuation) is dependent on proper phasing between the oscillating pressure and temperature. Rott showed that the oscillating temperature is linked to the pressure amplitude, to the acoustic impedance, and to the imposed temperature gradient, and identified the 'critical' temperature gradient, ∇T_c, above which acoustic power is generated. For an ideal inviscid gas, ∇T_c can be expressed as

$$\nabla T_c = \frac{\omega p_1}{\rho_m c_p u_1} \tag{1}$$

where $\omega.p_1, \rho_m c_p$ and u_1 are the angular frequency, oscillating pressure, mean density, heat capacity and oscillating velocity, respectively. Swift [12] developed Rott's theory further and designed several working thermoacoustic engines and refrigerators [17–19]. As illustrated in Fig. 1a, these engines rely on heat conduction between a gas and a solid "stack/regenerator"- a porous medium used to increase the effective volume of the gas in thermal contact with the solid (the interested reader can find an excellent account of classical thermoacoustics in Refs [1,12]). The stack/regenerator is an essential part of thermoacoustic devices, often referred to as the 'heart' of the device [1]. Early thermoacoustic engines supported a standing wave acoustic field, where the pressure and velocity oscillations are almost completely out of phase. A standing wave device requires stack pore sizes on the order of the thermal penetration depth, $\delta_\alpha = \sqrt{2\alpha/\omega}$, where α is the thermal

* Corresponding author.
E-mail address: ramong@technion.ac.il (G.Z. Ramon).

https://doi.org/10.1016/j.applthermaleng.2024.122915
Received 22 December 2023; Received in revised form 20 February 2024; Accepted 7 March 2024
Available online 15 March 2024

diffusivity of the gas and ω is the angular frequency of the acoustic wave. This leads to entropy generation due to imperfect thermal contact but is required for maintaining the exchange of heat necessary for amplifying and sustaining the oscillations. The inherent irreversibility substantially reduces the efficiency of standing wave engines, with efficiencies limited to ~20% of Carnot's efficiency [20,21].

The potential advantage of a traveling wave acoustic field was identified by Ceperley [22], who realized that the pressure–velocity phasing in a traveling wave is similar to that of a Stirling cycle. Pressure and velocity are in phase, in contrast to the situation in a standing wave engine, facilitating heat transfer at constant temperature, which offers the potential for significantly higher efficiency due to the reversible nature of isothermal heat transfer. However, accomplishing this requires excellent thermal contact, which dictates that the pore size be much smaller than the thermal penetration depth. While good thermal contact reduces thermal irreversibilities and has enabled the development of devices with significant power production, with efficiencies up to 40% of the Carnot efficiency [1,19,23–25], it possesses one significant drawback — smaller pores lead to substantial viscous losses. Modern thermoacoustic engines usually have complex topologies, aimed at increasing the acoustic Impedance to reduce viscous losses while maintaining a traveling wave phasing [25,26]. However, the problem is inherent and not fully solvable in this manner.

Therefore, to further improve the efficiency of thermoacoustic conversion, it is of interest to investigate alternative modes of energy transfer, where losses can be reduced. The generation of acoustic waves using radiation has been demonstrated in the bio-medical field, for photo-acoustic tomography (PAT) [27,28], where these waves are used for high-resolution, multi-scale imaging of body tissues. This demonstrates that radiation can be used to drive acoustic waves. Being volumetric in nature, such a mode of excitation can provide the means for converting heat to sound without the necessity of the solid intermediary – the stack/regenerator – and hence eliminate the main source of energy dissipation in the device. However, an important distinction is that photoacoustic oscillations are driven by an oscillating heat source (e.g., oscillating laser), while our proposed approach is based on a temporally-constant, but spatially non-uniform radiative field. These are, therefore, quite separate effects, albeit with a similar outcome. Qiu et al. [29] experimentally demonstrated thermoacoustic heat transfer mediated by such a radiative field, quantifying the interaction of acoustic and radiative fields and providing indication that radiation-driven thermoacoustic energy conversion is in fact possible. However, Their experiment did include an acoustic source and therefore did not demonstrate the spontaneous generation of an acoustic field from radiation.

It is, therefore, the aim of the present study to theoretically investigate the potential of radiation-driven thermoacoustic energy conversion in thermoacoustic engines, while identifying the underlying physics, and the conditions under which energy conversion may be enhanced.

2. Model formulation

Consider a Newtonian fluid contained within a cylindrical acoustic resonator with radius R and length L, as described in Fig. 1b. A cylindrical coordinate system is employed $(\hat{x}, \hat{r}, \theta)$, and the governing equations are the mass, momentum and energy balances,

$$\frac{D\hat{\rho}}{D\hat{t}} = -\hat{\rho}\nabla\cdot\hat{U}, \tag{2}$$

$$\hat{\rho}\frac{D\hat{U}}{D\hat{t}} = -\nabla\hat{p} + \nabla\cdot(\hat{\mu}\nabla\cdot\hat{U}), \tag{3}$$

$$\hat{\rho}\hat{T}\left(\frac{c_p}{\hat{T}}\frac{D\hat{T}}{D\hat{t}} - \frac{\hat{\beta}}{\hat{\rho}}\frac{D\hat{p}}{D\hat{t}}\right) = \hat{q} + \nabla(\hat{k}\nabla\hat{T}) + (\hat{\mu}\nabla\cdot\hat{U}) : \nabla\hat{U}, \tag{4}$$

in which a general volumetric heat source $\hat{q}(\hat{x}, \hat{T})$ is included, to represent the expected effect of radiation-induced heating. Here, $\hat{\rho}$ is the density, $\hat{U}$ is the velocity vector, $\hat{p}$ is the pressure, $\hat{T}$ the temperature and $\hat{t}$ is time. Further, $\hat{\mu}$ and $\hat{k}$ are the viscosity and thermal conductivity of the fluid, respectively, while $\hat{\beta}$ and $\hat{c_p}$ are the thermal expansion coefficient and the heat capacity, respectively. We also assume an ideal gas equation of state,

$$\hat{\rho} = \frac{\hat{p}}{R_g\hat{T}} \quad , \tag{5}$$

in which R_g is the substance's gas constant, i.e., the universal gas constant divided by the molar mass. With the additional assumptions of a calorically perfect gas ($c_p = const, \hat{\beta} = 1/\hat{T}$) Eq. (4) reduces to

$$\hat{\rho}c_p\frac{D\hat{T}}{D\hat{t}} - \frac{D\hat{p}}{D\hat{t}} = \hat{q} + \nabla(\hat{k}\nabla\hat{T}) + (\hat{\mu}\cdot\nabla\hat{U}) : \nabla\hat{U} \tag{6}$$

A concentrated light beam illuminates part of the resonator in the axial direction, and is absorbed by the fluid. The beam enters the resonator through a window, but the illuminated section of the resonator is assumed to be otherwise perfectly reflective, not allowing radiation to leave. This assumption is justified in the supplementary matrial to this work. Furthermore, we assume a gray, non-scattering media, a valid assumption for absorbing gases and aerosols of small particles, and is unrealistic for aerosols comprising large particles or droplets, such as clouds.[30] Under these assumptions, the radiative heat can be written as a volumetric heat source, of the form: [31],

$$\hat{q} = -\nabla q_r = 4\kappa\left(\pi\hat{\bar{I}} - \sigma\hat{T}^4\right), \tag{7}$$

where q_r is the radiative heat flux, κ is the absorption constant, $\hat{\bar{I}}$ is the radiation intensity, averaged over all wavelengths, and σ is the Stefan–Boltzmann constant. The mean radiation intensity, $\hat{I}$, should generally be obtained by solving the radiative transfer equation (RTE) in different directions. However, if the domain is perfectly insulated from radiation and heat transfer in the radial direction, the mean intensity is the axial component,

$$\bar{I} = I_x, \tag{8}$$

and the RTE in the axial direction is given as

$$\frac{d\hat{I}_x}{d\hat{x}} = -\kappa\hat{I}_x + \kappa\frac{\sigma\hat{T}^4}{\pi}. \tag{9}$$

Eq. (7) and (9) provide the full model for radiative heat transfer within the framework considered here. We note that the radiative properties of the fluid are of paramount importance, and will be discussed in Section 5.2.

2.1. The scaled equations

Next, we non-dimensionalize the model equations, using the following scaling substitutions [32],

$$x = \hat{x}/\lambda; \quad r = \hat{r}/R; \quad t = \omega\hat{t}; \quad U = \hat{U}/(\omega\lambda) \quad \rho = \hat{\rho}/\rho_0;$$
$$I = \hat{I}/(\rho_0\omega^3\lambda^3); \quad p = \hat{p}/(\rho_0\omega^2\lambda^2); \quad \mu = \hat{\mu}/\mu_0;$$
$$T = \frac{c_p}{\omega^2\lambda^2}\hat{T}; \quad \dot{q} = \hat{q}/(\rho_0\omega^3\lambda^2); \quad k = \hat{k}/k_0; \tag{10}$$

Here, $\omega = 2\pi a/\lambda$ is the angular frequency, with a denoting the speed of sound. Subscripts '0' denote reference values for different quantities, and the hat denotes a dimensional quantity. The final, non-dimensional form of Eq. (2)–(5) is then

$$\frac{\tilde{D}\rho}{\tilde{D}t} = -\rho\tilde{\nabla}\cdot U, \tag{11}$$

$$\rho\frac{\tilde{D}U}{\tilde{D}t} = -\tilde{\nabla}p + \frac{1}{\tau_{v_0}^2}\tilde{\nabla}\cdot(\mu\tilde{\nabla}\cdot U), \tag{12}$$

$$\rho\frac{\tilde{D}T}{\tilde{D}t} - \frac{\tilde{D}p}{\tilde{D}t} = \dot{q} + \frac{1}{\tau_{\alpha_0}^2}\nabla(k\nabla T) + \frac{1}{\tau_{v_0}^2}(\mu\cdot\tilde{\nabla}U) : \tilde{\nabla}\cdot U, \tag{13}$$

$$\rho = \frac{\gamma}{\gamma-1}\frac{p}{T}, \tag{14}$$

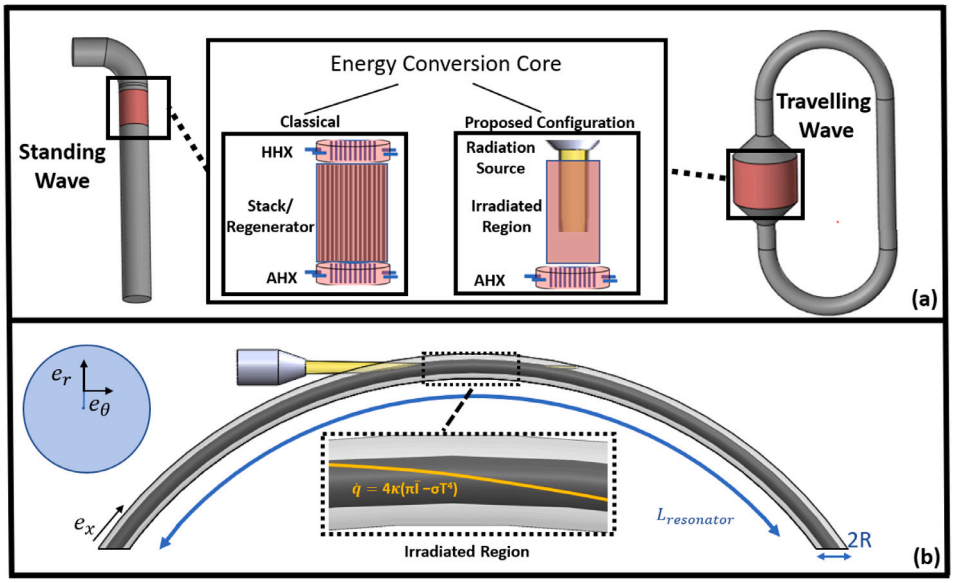

Fig. 1. **(a)** Schematic of typical standing wave and traveling wave thermoacoustic engines. Energy conversion occurs in the "energy conversion core". In classical thermoacoustic systems, this is a stack/regenerator (porous media) over which a temperature gradient is imposed. In a radiation-driven engine, the stack/regenerator is replaced by an irradiated region. **(b)** Schematic of our modeled geometry — an acoustic resonator irradiated by a light beam. In the irradiated region, a spatially non-uniform volumetric heat source $\dot{q}$ is created.

and the form of Eq. ((7) and (9)) is:

$$\dot{q} = 4\kappa^* \left(\pi\bar{I} - \sigma^* T^4\right), \tag{15}$$

$$\frac{dI_x}{dx} = -\kappa^* I_x + \kappa^* \frac{\sigma^* T^4}{\pi}, \tag{16}$$

Respectively. the scaled operators are defined as

$$\tilde{\nabla} = \frac{\partial}{\partial r} e_r + \frac{\partial}{\partial \theta} e_\theta + \frac{R}{\lambda} \frac{\partial}{\partial x} e_x, \tag{17}$$

$$\frac{\tilde{D}}{\tilde{D}t} = \frac{R}{\lambda} \frac{\partial}{\partial t} + U \cdot \tilde{\nabla}. \tag{18}$$

Here, e_i is the unit vector in direction i, $\tau_{v_0} = R\sqrt{\omega/v_0}$ and $\tau_{\alpha_0} = R\sqrt{\omega/\alpha_0}$ represent the scaled conduction and viscous times, and γ is the specific heat ratio. Lastly, $\kappa^* = \kappa\lambda$ and $\sigma^* = \sigma\omega^5\lambda^5/\rho_0 c_p^4$ are the scaled absorption coefficient and Stephan-Boltzmann constant, respectively.

3. Derivation of the 1D wave equation

Next, we proceed to derive the equations governing the radiation-driven thermoacoustic waves, which form the basis for the forthcoming analysis. The governing equations are manipulated into a single ODE - a 1D wave equation. We follow [32] and assume all variables are time-harmonic, of the form

$$g = g_m + \Re\left(g_1 e^{it}\right), \tag{19}$$

in which $g_1 \ll g_m$, such that the subscript m represents a time-averaged quantity and the subscript 1 denotes an oscillating property. The velocity, u, consists only of the oscillating part u_1, and satisfies $u_1 \ll 1$. In addition, we assume $L_{resonator} \gg R$, axisymmetry and negligible conduction (in the configuration considered, axial conduction is small since $R \ll \lambda$, and in the radial direction it can be neglected when $\tau_\alpha \gg 1$). With these assumptions, Eq. (12)–(13) may be written as

$$\frac{ip_1}{p_m} - \frac{iT_1}{T_m} - \frac{u_1}{T_m}\frac{dT_m}{dx} + \frac{du_1}{dx} = 0, \tag{20}$$

$$u_1 = i\frac{F_v}{\rho_m}\frac{dp_1}{dx}, \tag{21}$$

$$\rho_m i T_1 - i p_1 + \rho_m u_1 \frac{dT_m}{dx} = \dot{q}_1, \tag{22}$$

where

$$F_v = 1 - \frac{J_1[(1-i)\tau_v]}{J_0[(1-i)\tau_v][(1-i)\tau_v]}. \tag{23}$$

Here, $u = \langle U \cdot e_x \rangle$ is the cross-sectional-averaged axial velocity, and J_n represents the nth-order Bessel function of the first kind. In addition, under the same asymptotic conditions, $u_m = 0$, $u_r = 0$, $p_m = p_m(x)$ and $\dot{q}_m = 0$.

Eq. (15) becomes

$$\dot{q}_1 = 4\kappa^* \left(\pi\bar{I} - \sigma^*(T_m + T_1)^4\right), \tag{24}$$

and we separate this equation into a mean and time-dependent part, while neglecting terms of order $O(T_1)^2$:

$$\dot{q}_1 = -16\kappa^*\sigma^* T_m^3 T_1, \tag{25}$$

$$\pi\bar{I} = \sigma^* T_m^4 \tag{26}$$

with which Eq. (22) reduces to

$$T_1 = \frac{p_1 + i\rho_m u_1 \frac{dT_m}{dx}}{\rho_m - 16i\kappa^*\sigma^* T_m^4}. \tag{27}$$

Combining Eqs. (20)–(21), along with (14) and (27), results in a single ordinary differential equation,

$$A_0 p_1 + A_1 \frac{dp_1}{dx} + A_2 \frac{d^2 p_1}{dx^2} = 0 \tag{28}$$

Where

$$A_0 = \frac{i}{\gamma - 1} + \frac{16\kappa^*\sigma^* T_m^4}{p_m},$$

$$A_1 = \left(\frac{\gamma p_m}{\gamma - 1} - 16\kappa^*\sigma^* T_m^4\right)\frac{d}{dx}\left(\frac{iF_v}{\rho_m}\right) - \frac{16\kappa^*\sigma^* T_m^3 F_v}{\rho_m}\frac{dT_m}{dx},$$

$$A_2 = \left(\frac{\gamma}{\gamma - 1} p_m - 16\kappa^*\sigma^* T_m^4\right)\frac{iF_v}{\rho_m}.$$

This is a wave equation for the oscillating pressure p_1. Given a known mean temperature profile, along with appropriate boundary conditions, this equation can be solved numerically.

4. Periodic regime analysis

The periodic regime analysis, based on Eq. (28), is achieved by solving for the mean temperature, oscillating pressure, and oscillating velocity fields under varying conditions corresponding with a specific heat input. The configuration considered is a 1D resonator with either a traveling wave or standing wave acoustic field, as displayed in Fig. 1a. The periodic regime solution is then used to compute the predicted performance of radiation-driven thermoacoustic devices, in terms of efficiency and power density. To better account for losses commonly found in such systems, conduction within the surrounding solid wall of the resonator is added to the energy balance. In our analysis, heat is introduced into the system using radiation, while the ambient end of the irradiated region is fixed at the ambient temperature, which is equivalent to assuming an ideal heat-exchanger. We note that practial configurations would require an ambient heat exchanger, which will add some viscous losses to the system, as well as imperfect heat transfer.

4.1. Total power

The total power flux in the axial direction may be written as

$$\hat{\dot{H}} = \hat{\rho_m} c_p \cdot \left(\pi R^2 \frac{1}{2} Re(\hat{u_1}\hat{T_1}) - \hat{\alpha_s} A_s \frac{d\hat{T_m}}{d\hat{x}} - \pi R^2 \frac{16\sigma \hat{T_m}^3}{3\kappa \hat{\rho_m} c_p} \frac{d\hat{T_m}}{d\hat{x}} \right), \tag{29}$$

where $\hat{\dot{H}}$ is the total power transported in the irradiated segment due to hydrodynamic dispersion, conduction in the solid part of the tube, and radiation within the absorbing media. Here, $\hat{\alpha_s}$ and A_s are the thermal diffusivity and cross-sectional area of the solid resonator section, respectively. We note that the first and second terms in Eq. (29) are known in the thermoacoustics literature (e.g., [1,12]) and the last term is a textbook result for radiative transfer within absorbing media, in the absence of flow [31]. Lastly, the scaled total power and diffusivity are defined as $\dot{H} = \hat{\dot{H}} / \left(\rho_0 \omega^3 \lambda^3 R^2\right), \alpha_s = \hat{\alpha_s} / \left(\lambda^2 \omega A_g / A_s\right)$, such that

$$\dot{H} = \pi \rho_m \left(\frac{1}{2} Re\left(\tilde{u_1} T_1\right) - \alpha_s \frac{dT_m}{dx} - \frac{16\sigma^* T_m^3}{3\rho_m \kappa^*} \frac{dT_m}{dx} \right) \tag{30}$$

is the equation for the scaled total power. With a known temperature profile, Eq. (30) can be used to estimate the amount of power that will be transported down the temperature gradient by the acoustic field. Alternatively, it can be used to solve for the temperature gradient required to transfer a known amount of energy, as will be done in the following section.

4.2. Methodology

To perform the periodic regime analysis, Eq. (27) is substituted into Eq. (30) and manipulated into a differential equation for T_m. This equation is coupled with the wave equation (Eq, (28)) and both are solved simultaneously for the distributions of p_1, u_1, and T_m. Both traveling wave ($L \approx 1$, $p_1(0) = p_1(L)$, $u_1(0) = u_1(L)$) and standing wave ($L \approx 1/2$, $u_1(0) = u_1(L) = 0$) configurations are considered (a schematic of these configurations can be seen in Fig. 1a). In the non-irradiated segments, the standard acoustic propagation equations are solved, accounting for thermal relaxation, viscous dissipation, and, where appropriate, turbulent losses [1] (The full set of equations is provided in the supplementary material to this work).

All the equations were solved using a variable order Runga-Kutta method with a hybrid Powell shooting method, implemented within our in-house solver - PC-TAS, a simulation software for 1D acoustics and thermoacoustics (for further details, see ref [33]). The working fluid considered is air at a pressure of 10 bar, however, in order to facilitate a simple variation of the radiation absorptivity, κ was assumed independent of the material properties, and was modified so as to probe the effect of τ_σ on system performance. We note that, in a physical realization of the system considered here, absorptivity could be modified by the introduction of aerosols into the fluid, or by matching the radiation wavelength with fluid absorption lines (for example, by crafting an appropriate mixture such as SF_6 and air, irradiated with a CO_2 laser at a wavelength of $\tilde{1}0$ μm). Either of these variations might affect other fluid properties (viscosity, density, etc.) considerably. However, for the purpose of the present analysis, aimed at gaining basic insight into this configuration, we neglect these effects for the sake of (relative) simplicity. In the calculations, the dimensional ambient temperature, $\hat{T_a}$, was kept constant at 400 K, while the hot temperature $\hat{T_H}$ was varied between 500-600K. Additional geometrical features, such as the location of the irradiated segment inside the resonator, the aspect ratio of the system, as well as the length of the irradiated segment, were roughly iterated via trial and error to improve system performance, but the system is not optimized. In the traveling wave system, the irradiated segment was assumed wider than the non-irradiated segments (exact dimensions can be found in the supplementary material), to increase the acoustic impedance, p_1/U_1, of the sound wave in the irradiated region. This is common practice in traveling wave thermoacoustics [34–36], and indeed improved performance in the case presented here, as well. It is important to note that the total radiative power input into the system was set as a guess, targeting the prescribed hot temperature that corresponds with this amount of power. Thus, a non-linear temperature profile was created inside the irradiated section, corresponding with a constant value of the total power, $\dot{H}$ (see Eq. (30)). The produced power is found by calculating the difference between acoustic power on both sides of the irradiated segment. Efficiency was calculated by dividing the produced power by the total power, $\dot{H}$, within the irradiated segment. Additional details about the periodic regime analysis can be found in the supplementary material to this work.

5. Results and discussion

5.1. Simplified model

We begin with a simplified analysis, in an attempt to gain insight regarding the conditions under which radiation-driven thermoacoustic conversion is expected to occur. In particular, we will illustrate that any non-uniform, temperature-dependent heat source has the potential to generate acoustic power. To this end, we neglect viscous losses, thermal conductivity, and any two-dimensional effects present. Most importantly, the effect of the heat source on the wave itself is ignored, which means that the density in Eqs. (11) and (12) is dependent only on the pressure. Strictly speaking, this assumption is valid only for very small temperature variations. However, it is very useful because it decouples Eq. (13) from Eq. (11)–(12), permitting an analytical solution. We note that all of the assumptions made in this subsection are made in order to facilitate the present discussion, whereas in the following segment, (Section 5.2), the discussion is based on the full model.

As in the classical derivation of the acoustic wave equation, we seek a solution for a small disturbance $p' \ll p_m$ where p_m is the mean pressure, and solve Eqs. (11)–(12) with a no penetration boundary condition ($U = 0$) at $x = 1/4$ and with a symmetry boundary condition ($p' = 0$) at $x = 0$. The solution is a simple, ideal acoustic standing wave, in the domain $0 < x < \frac{1}{4}$:

$$p = p_m + \Re\left(p_a \sin(2\pi x) e^{it}\right), \tag{31}$$

$$U = \Re\left(i p_a \cos(2\pi x) e^{it}\right), \tag{32}$$

where $\Re$ represents the real part of a complex number. Under the given assumptions, Eq. (13) reduces to

$$\rho \frac{dT}{dt} - \frac{dp}{dt} + U\left(\rho \frac{dT}{dx} - \frac{dp}{dx}\right) = \dot{q}. \tag{33}$$

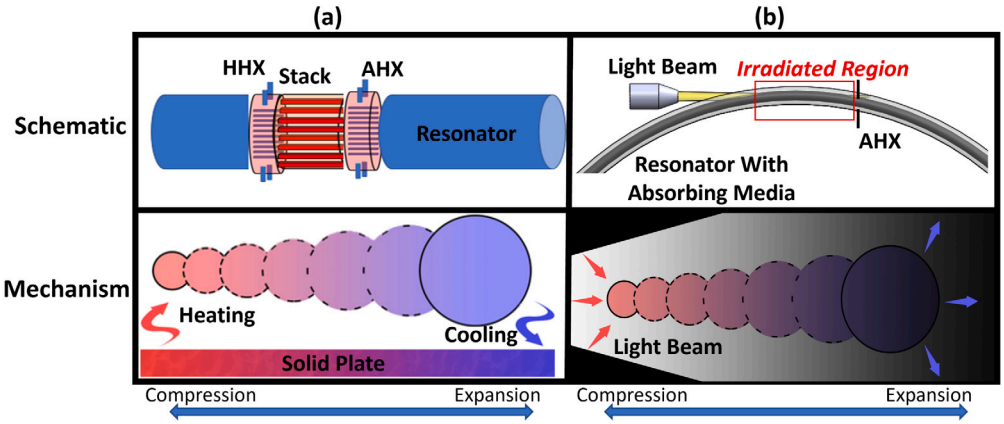

Fig. 2. Schematic (top) and energy conversion mechanism (bottom) in **(a):** a classical thermoacoustic engine, with a stack (porous media) and **(b):** proposed configuration with a non-uniform radiative field. In both cases, energy conversion is related to proper phasing between compression, expansion and heat transfer to and from the gas. In the presence of a non-uniform radiative field, the gas absorbs radiation in the irradiated region, and expels radiative heat in the "dark region" (i.e. the region with a weaker radiative field). Net heat is transported down the temperature gradient.

We introduce a volumetric heat source, of the form

$$\dot{q} = A(x) - B(x)T, \tag{34}$$

in which A and B are some functions of X. The addition of a temperature-dependent term to the heat source is at the heart of the proposed thermoacoustic mechanism. In the present analysis, a linear dependency was assumed for the sake of simplicity.

Next, the temperature, like the pressure and velocity, is assumed to take the form

$$T = T_m + \Re\left(T_1 e^{it}\right) \qquad T_1 \ll T_m. \tag{35}$$

Expanding and retaining zeroth and first-order terms, we have the solutions for T_m and T_1 respectively,

$$T_m = \frac{A}{B} \tag{36}$$

$$T_1 = \frac{\rho_m p_a \left(\sin(2\pi x) - \rho_m \frac{dT_m}{dx}\cos(2\pi x)\right)}{B^2 + \rho_m^2} + \tag{37}$$

$$i\,\frac{B p_a \left(\sin(2\pi x) - \rho_m \frac{dT_m}{dx}\cos(2\pi x)\right)}{B^2 + \rho_m^2}. \tag{38}$$

These expressions point out several aspects. First, in the absence of a heat source, the sound wave is adiabatic and the solution reduces to the known oscillatory temperature in an adiabatic sound wave,

$$T_1 = T_m \frac{\gamma - 1}{\gamma}\frac{p_1}{p_m}, \tag{39}$$

where p_1 is the oscillatory pressure. We note that Eq. (36) is not valid in the adiabatic case, for which any constant value of T_m is valid. Importantly, we see that the presence of a heat source leads to an imaginary part of T_1, meaning that the temperature is no longer in phase with the pressure. This is important since the existence of an imaginary part of T_1 leads to absorbed or generated acoustic power per unit volume, which can be estimated as [12]

$$\hat{\dot{w}} = -\frac{1}{2}\omega \frac{\hat{p_a}\sin\left(\frac{2\pi\hat{x}}{\lambda}\right)}{\hat{T_m}} Im(\hat{T_1}), \tag{40}$$

with the sign of $\hat{\dot{w}}$ indicative of whether acoustic power is generated or absorbed by the thermal interaction. The acoustic power is scaled based on

$$\dot{w} = \frac{\hat{\dot{w}}}{\rho_0 \omega^3 \lambda^2}, \tag{41}$$

Table 1
Summary of the two cases in Section 5.1, their heating profiles and resultant temperature profiles and acoustic power. These results are shown quantitatively in figure 3.

Case	1	2
Heating profile	Uniform	Non-uniform
Resulting temperature profile	Uniform	Non-uniform, critical temperature gradient present
Acoustic power	Consumed only	consumed when $\nabla T < \nabla T_c$ produced when $\nabla T > \nabla T_c$

yielding

$$\dot{w} = -\frac{1}{2}\frac{p_a \sin(2\pi x)}{T_m} Im(T_1). \tag{42}$$

Finally, we note that there is a critical temperature gradient in our solution, where the acoustic power transitions from negative to positive,

$$\nabla T_{crit} = \frac{p_1}{\rho_m U_1} = \frac{\sin(2\pi x)}{\rho_m \cos(2\pi x)}, \tag{43}$$

which corresponds with the 'critical gradient' as defined in classical thermoacoustics [12]. However, in our case, this is a result of a volumetric heat source, rather than interaction with a solid surface. The analogy between both cases is shown in Fig. 2, which illustrates the energy conversion mechanism in the classical and radiation-driven configurations. In all cases, energy conversion occurs due to the heating of the fluid when it is compressed and cooling it when it is expanded. While the heat source in classical thermoacoustic engines is a solid surface, it can in fact be any sort of temperature-dependent heat source. Eq. (36) indicates that the temperature distribution is a direct outcome of the way the heat source is distributed. Therefore, gradients in the volumetric heat source can lead to temperature gradients. If these gradients are steep enough, the critical temperature gradient will be exceeded, and acoustic power will be generated. The different cases are summarized in Table 1.

Next, we examine solutions for two different heating profiles, characterized by the functions A(x) and B(x) in Eq. (34) (see Fig. 3). The two heating profiles, chosen for the purpose of illustration, represent the cases of uniform heat generation, and intense heating at a specific location inside the resonator, as can be seen in the inset of Fig. 3. For both cases, the mean pressure was set to unity, the scaled pressure amplitude is set to 0.05, and the specific heat ratio is 1.4. In order to validate the simplified, linear model, Eq. (33) was also solved directly, using an upwind numerical scheme with time integration performed

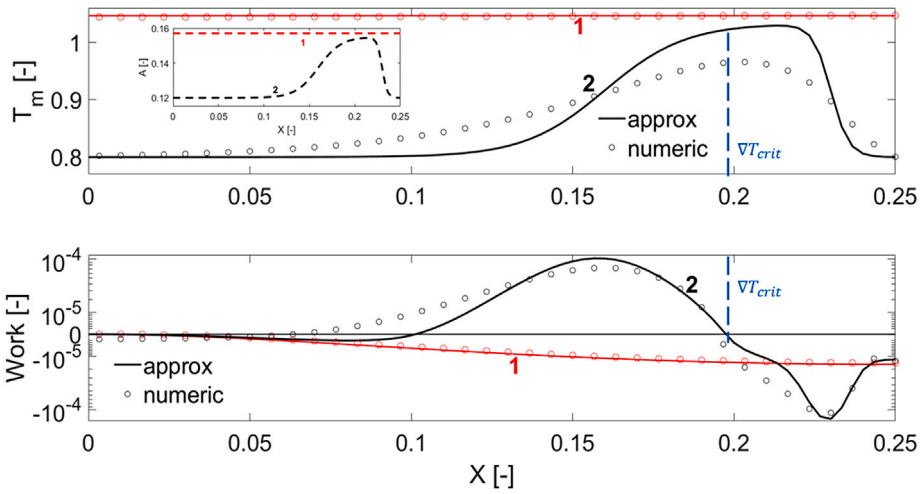

Fig. 3. Calculated mean temperature (top) and generated acoustic power (bottom) for two different heating profiles of the form $\dot{q} = A - BT$. For both cases B was selected to be constant (0.15) in the entire resonator, while A varies as displayed in the inset figure. Case 1 describes a uniform heat generation profile and case 2 a highly non-uniform one. The mean temperature and work in each case are solved for via the acoustic approximation (Eq. (38)–(42)). Note that work in case 1 is purely negative while work in case 2 changes from positive to negative when passing a critical temperature gradient (marked in the figure by the dashed vertical line labeled ∇T_{crit}, defined by Eq. (43)).

using a two-stage Runge–Kutta method, with the discretization steps for t and x taken as $\frac{1}{2000}$ and $\frac{1}{300}$, respectively. The solution was time-averaged so as to evaluate the mean temperature, and the acoustic work was calculate by [12]

$$\dot{w} = \overline{\frac{p}{\rho_m}\frac{\partial \rho}{\partial t}}. \tag{44}$$

The calculations of the mean temperature profile are presented in Fig. 3, demonstrating good agreement between the linear and non-linear models, with slight deviations seen in case 2, especially in the locations where the linear model predicts strong gradients. The deviation may be attributed to higher order effects, and specifically acoustic streaming, which is known to be stronger in the presence of sharp gradients [1]. The agreement is quite good in the limit of small amplitudes ($p_1/p_m \ll 1$), where non-linearities are inherently small.

The calculated acoustic work is presented in the bottom of Fig. 3. In the first case, of uniform heat generation, the acoustic power is negative within the entire domain — this means the system is purely dissipative. This is similar to the introduction of an isothermal plate into an acoustic wave, which leads to thermal relaxation [1], therefore, we expect the acoustic wave to be attenuated. In the second case the acoustic power changes from negative to positive when the temperature gradient passes a critical value, at a given spatial position (marked as ∇T_{crit} in the figure). At this point, the generated acoustic power is of the same order of magnitude as the viscous dissipation ($O(p_a)^2$), such that acoustic oscillations are sustained or amplified.

The conclusion from this illustrative analysis is that not all volumetric heat sources can generate acoustic amplification. However, a non-uniform and, more importantly, temperature-dependent heat source can lead to generation of acoustic power, the magnitude of which depends on the sharpness of the gradient, and on the location of the heat source within the acoustic field.

If acoustic power is indeed generated, an acoustic disturbance is expected to grow until the various dissipation mechanisms (mostly viscosity and thermal relaxation) counter the power generated by the thermoacoustic amplification. Finally, we note that Eq. (15) demonstrates that any non-uniform profile of $\overline{I}$ will result in a temperature dependent, non-uniform heat source, and can therefore potentially trigger an instability. In other words, it is shown that a non-uniform radiative field can drive a thermoacoustic instability. The energy conversion mechanism is presented in 2 (b): in the absence of an acoustic field, a non-uniform radiative field leads to a corresponding temperature gradient, with higher temperatures in the area closer to the radiation source. A thermal equilibrium is reached, where the gas radiates as much radiation as it absorbs at each point. If an acoustic disturbance is introduced, the thermal equilibrium is upset: When a parcel of gas moves slightly toward the irradiated region, it absorbs net heat, and when it moves to the "darker" region (further from the source of radiation), it emits heat. This leads to net heat transport down the temperature gradient, as has been experimentally observed by Qiu [29]. However, it can also lead to conversion of thermal energy to acoustic energy, i.e., amplification of the acoustic wave, as shown here.

5.2. Periodic regime results

In this section, we discard the simplifying assumptions of Section 5.1, and display results from full solution of the wave equation. Calculations of the periodic regime indicated that performance, in terms of power produced, depends strongly on absorptivity, κ. In a standing acoustic wave, the absorptivity should allow for comparable characteristic time scales for the oscillation, $1/\omega$, and heating, $\hat{\rho}c_p/4\kappa\sigma\hat{T}^3$. This is similar to the requirement in traditional thermoacoustic systems, for a comparable scale between the oscillation time and the thermal diffusion characteristic time $\hat{\alpha}/y_0^2$ (where $\hat{\alpha}$ is the thermal diffusivity of the fluid and y_0 is a typical pore size (see, e.g., [12,16]). We define the parameter

$$\tau_\sigma = \frac{\omega\hat{\rho}c_p}{4\kappa\sigma\hat{T}^3} = \frac{\rho}{4\kappa^*\sigma^*T^3}, \tag{45}$$

representing the ratio of the characteristic heating time and oscillation time in a radiation-driven system. The calculated efficiency of heat-to-acoustic power conversion (relative to Carnot's limit - $\eta_r = \eta/\eta_C$) and power density are shown in Fig. 4, for both standing wave and traveling wave configurations, as a function of the hot temperature, $\hat{T_H}$, and of τ_σ.

The results demonstrate high power densities and excellent efficiencies for standing and, particularly, traveling wave devices. The efficiency of the traveling wave engine is much higher than that of the standing wave engine. This is an expected result, related to the inherent irreversibility of the thermodynamic cycle in standing wave engines. A comparison to classical thermoacoustic engines is warranted. We note that comparison to a conduction-driven device with the same geometry could be considered unfair, due to the geometry not being necessarily optimal for classical engines. The same could be said for comparison of our performance predictions, which are based on a simplified model,

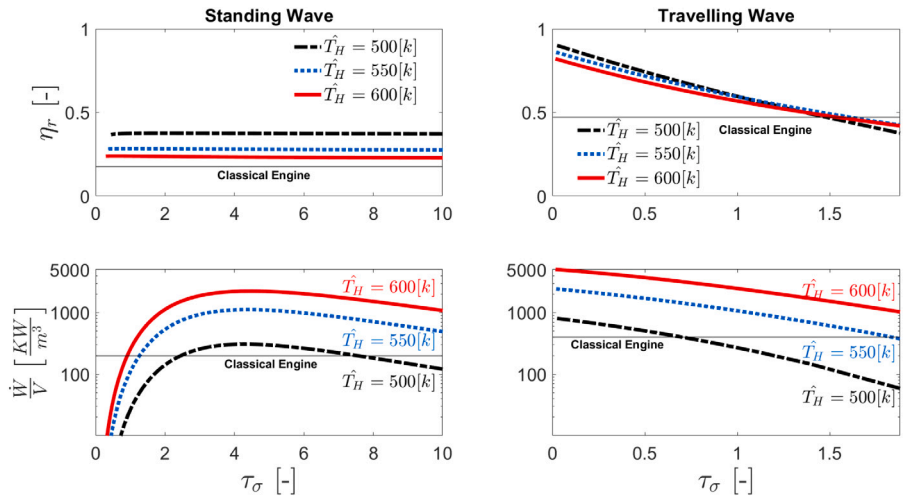

Fig. 4. Periodic regime results from the linear model for a standing and traveling wave systems (see Fig. 1 **(a)**). Efficiency (Top) varies between 0.2–0.9 of Carnot's efficiency. Power density (bottom) can reach up to 5 [MW/m^3]. Optimal value of the scaled characteristic time is $\tau_\sigma \approx 4$ for standing wave engines (poor "thermal contact" allowing for temperature variations within the radiative field) and $\tau_\sigma \to 0$ for a traveling wave engine (excellent "thermal contact" imposing near isothermal temperature conditions). A comparison to results from a similar model for a classical thermoacoustic engine (see supplementary material for details) is supplied.

with performance of actual working thermoacoustic engines. Therefore, we chose to make the comparison with state-of-the-art results based on a similar model: The 1D linear model for thermoacoustic engines as proposed by [16] and extended by [12]. This model, based on similar assumptions to our model here (single frequency oscillations, 1D propagation, low amplitudes) is used for optimization and performance prediction. It often overpredicts performance [17,37], but provides good estimations. For comparison, we ran simulations of a stack and a regenerator under an ideal standing and traveling field, respectively. Resonator losses were neglected, and the length, pore size, and acoustic impedance were very roughly optimized. Additional details of the linear model simulation can be found in the supplementary material.

As can be seen in Fig. 4, and despite the favorable conditions in the classical engine, the radiation-driven engine outperforms it in both efficiency and energy density. The classical engine results presented in Fig. 4 are with a hot temperature of 550 [K]. Results with different hot temperatures are presented in the supplementary material. The dependence of the performance on τ_σ is substantial. As expected, standing wave devices achieve maximum performance at around $\tau_\sigma \approx 1$ (4, to be exact, in the case considered), and traveling wave devices at around $\tau_\sigma \to 0$. This is due to the nature of the thermodynamic cycles mimicked within the different acoustic fields, and is analogous to conduction-driven devices, in which $\tau_\alpha \approx 3$ and $\tau_\alpha \to 0$ for standing and traveling wave devices, respectively (see [1]). We note that second-law efficiency is inversely proportional to the temperature in both devices. This is a known results in thermoacoustic engines, and relates to increased thermal irreversibilities. [12].

While the model predictions are very encouraging, both in terms of illustrating the very prospect of radiation-driven thermoacoustic energy conversion, as well as the projected performance of devices implementing this mode of energy conversion, several model limitations must be noted, as they likely lead to performance over-prediction. First, the assumption of a gray medium is made, such that all spectral effects are neglected, as is scattering. Such effects could potentially hamper the performance of these devices, but they cannot be accounted for without knowledge of the actual absorbing media or radiation source. However, in certain absorbing media (i.e very small dense suspended particles) spectral effects are negligible, and the scattering coefficient can be smaller than the absorption coefficient by several orders of magnitude [31]. Second, no acoustic load was imposed on the system, and all of the generated acoustic power was dissipated by the resonator. In reality, the acoustic power will be consumed (e.g, by a thermoacoustic heat pump or acoustic-electric transducer), and resonator losses will be reduced but not eliminated. Separately accounting for the produced acoustic power within the irradiated segment and the power extracted from the system will reduce the calculated efficiency and power density by about 5%–10% [18]. Further, the mechanisms of heat extraction from the ambient side were not addressed in this model. Any sort of heat exchanger will probably require a lower actual ambient temperature and in addition might add some viscous attenuation of the acoustic wave. In addition, the assumption of 1D radiation propagation is only valid if the irradiated section is a perfect radiation cavity, i.e, if the resonator walls are perfectly reflective. While near-perfectly reflective materials exist, they are often difficult to implement in high temperature and pressure environments. A reflectivity smaller than 80% (i.e polished aluminum) might cause substantial deviation from the model presented here. Finally, The effects of turbulence and heat conduction in the irradiated region, as well as various non-linear mechanisms (e.g streaming) were not addressed by the model presented here, and may become important at high amplitudes. We also note that neglecting thermal conductivity, while keeping viscous terms, is somewhat unjustified, seeing that the Prandtl number of most fluids is of order 1. This was done to simplify the equations considerably, while keeping some dissipation mechanism in the equations. Both effects are taken into account in the un-irradiated section, which amounts to most of the length of the system.

6. Concluding remarks

In this work, a radiation-driven mode of thermoacoustic instability was examined theoretically. Employing a simplified model, it was demonstrated how any non-uniform, temperature-dependent heat source can cause generation of acoustic power in a standing acoustic wave. Such sources include, but are not limited to, irradiation of a medium. Indeed, the framework presented here might be used to investigate any kind of volumetric heat source, including combustion, nuclear or chemical reactions, or the spaced-averaged effect of a "classical" conduction driven thermoacoustic system.

A more elaborate model was then used to derive a wave equation, describing the acoustic field. A periodic regime analysis demonstrated the potentially superior performance of radiation-driven thermoacoustic devices over classical devices. Results indicated that reasonable performance depends heavily on matching the characteristic heating time with the acoustic oscillation period. Such matching requires highly absorbing media, for example, atmospheric air at a mean temperature of 700 K will require $\kappa \approx 10,000$ for $\tau_\sigma = 1$. Therefore, experimental

demonstration of this phenomenon in future research will require methods for increasing the working media's absorptivity. A leading option for this could include particulate aerosols that can have significant absorptivity without greatly affecting the fluid properties [30]. Other options include supercritical fluids and compressible liquids. Analysis of such fluids will require modification of our model, which is based on an ideal gas assumption. However, for the sake of simplicity and in order to isolate the effect of radiation as much as possible, we chose to present the model in its current form, so as to motivate future expansions of this concept.

CRediT authorship contribution statement

Nathan Blanc: Writing – review & editing, Writing – original draft, Methodology, Formal analysis, Conceptualization. **Guy Z. Ramon:** Writing – review & editing, Supervision, Methodology.

Declaration of competing interest

The authors declare that they have no known competing financial interests or personal relationships that could have appeared to influence the work reported in this paper.

Data availability

Data will be made available on request.

Acknowledgments

The research was funded by the Israel Ministry of Energy and Infrastructure, grant 222-11-051. N.B Would like to thank the Grand Technion Energy Program (GTEP) for their support. The authors wish to thank Carmel Rothschild and Adam Dvir for insightful discussions, and Sagi Zaid-Or for his assistance with the illustration.

Appendix A. Supplementary data

Supplementary material related to this article can be found online at https://doi.org/10.1016/j.applthermaleng.2024.122915.

References

[1] G. Swift, Thermoacoustics - A Unifying Perspective for Some Engines and Refrigerators, Springer, 2002.
[2] A. Meir, A. Offner, G.Z. Ramon, Low-temperature energy conversion using a phase-change acoustic heat engine, Applied Energy 231 (2018) 372–379.
[3] G. Chen, L. Tang, B.R. Mace, Modelling and analysis of a thermoacoustic-piezoelectric energy harvester, Appl. Therm. Eng. 150 (2019) 532–544.
[4] J. Xu, E. Luo, S. Hochgreb, Study on a heat-driven thermoacoustic refrigerator for low-grade heat recovery, Appl. Energy 271 (2020) 115–167.
[5] J. Chi, Y. Yang, Z. Wu, R. Yang, P. Li, J. Xu, L. Zhang, J. Hu, E. Luo, Numerical and experimental investigation on a novel heat-driven thermoacoustic refrigerator for room-temperature cooling, Appl. Therm. Eng. 218 (2023) 119330.
[6] N. Weiland, B. Zinn, Open cycle traveling wave thermoacoustics: Energy fluxes and thermodynamics, J. Acoust. Soc. Am. 116 (2004) 1507.
[7] M. Tijani, S. Spoelstra, A hot air driven thermoacoustic-stirling engine, Appl. Therm. Eng. 61 (2) (2013) 866–870.
[8] K. Wang, S. Dubey, F.H. Choo, F. Duan, Thermoacoustic stirling power generation from LNG cold energy and low-temperature waste heat, Energy 127 (2017) 280–290.
[9] Z. wu, W. Dai, M. Man, E. Luo, A solar-powered traveling-wave thermoacoustic electricity generator, Sol. Energy 86 (2012) 2376.
[10] J.A. Adeff, T.J. Hofler, Design and construction of a solar-powdered, thermoacoustically driven, thermoacoustic refrigerator, J. Acoust. Soc. Am. 107 (6) (2000) L37–L42.
[11] C. Shen, H.-X. Li, D.-W. Zhang, P. Yu, N. Pan, S.-F. Wang, Study on the heat transfer characteristic of solar powered thermoacoustic prime mover at different tilted angles, Appl. Therm. Eng. 103 (2016) 1126–1134.
[12] G.W. Swift, Thermoacoustic engines, J. Acoust. Soc. Am. 84 (4) (1988) 1145–1180.
[13] A.C. Trapp, F. Zink, O.A. Prokopyev, L. Schaefer, Thermoacoustic heat engine modeling and design optimization, Appl. Therm. Eng. 31 (14–15) (2011) 2518–2528.
[14] C. Sondhauss, Ueber die Schallschwingungen der Luft in erhitzten Glasr hren und in gedeckten Pfeifen von ungleicher Weite, Ann. Phys. 155 (1) (1850) 1–34.
[15] P.L. Rijke, Notiz über eine neue Art, die in einer an beiden Enden offenen Röhre enthaltene Luft in Schwingungen zu versetzen, Ann. Phys. 183 (6) (1859) 339–343.
[16] N. Rott, Thermally driven acoustic oscillations. Part II: Stability limit for helium, Z. Angew. Math. Phys. 24 (1) (1973) 54–72.
[17] G.W. Swift, Analysis and performance of a large thermoacoustic engine, J. Acoust. Soc. Am. 92 (3) (1992) 1551–1563.
[18] S. Backhaus, G.W. Swift, A thermoacoustic-Stirling heat engine: Detailed study, J. Acoust. Soc. Am. 107 (6) (2000) 3148–3166.
[19] S. Backhaus, G.W. Swift, A thermoacoustic stirling heat engine, Nature 399 (6734) (1999) 335–338.
[20] A. Migliori, G.W. Swift, Liquid-sodium thermoacoustic engine, Appl. Phys. Lett. 53 (5) (1988) 355–357.
[21] L. Liu, P. Yang, Y. Liu, Comprehensive performance improvement of standing wave thermoacoustic engine with converging stack: Thermodynamic analysis and optimization, Appl. Therm. Eng. 160 (2019) 114096.
[22] P.H. Ceperley, A pistonless Stirling engine—The traveling wave heat engine, J. Acoust. Soc. Am. 66 (5) (1979) 1508–1513.
[23] T. Bi, Z. Wu, L. Zhang, G. Yu, E. Luo, W. Dai, Development of a 5kW traveling-wave thermoacoustic electric generator, Appl. Energy 185 (2017) 1355–1361.
[24] K. Tang, Y. Feng, T. Jin, S. Jin, M. Li, R. Yang, Effect of gedeon streaming on thermal efficiency of a travelling-wave thermoacoustic engine, Appl. Therm. Eng. 115 (2017) 1089–1100.
[25] L. Liu, Y. Liu, F. Duan, Effect of the characteristic time on the system performance of a three-stage looped traveling-wave thermoacoustic engine, Energy Convers. Manage. 224 (2020) 113367.
[26] A. Al-Kayiem, Z. Yu, Numerical investigation of a looped-tube travelling-wave thermoacoustic engine with a bypass pipe, Energy 112 (2016) 111–120.
[27] J. Yao, L.V. Wang, Photoacoustic tomography: fundamentals, advances and prospects, Contrast Media Mol. Imag. 6 (5) (2011) 332–345.
[28] A.B.E. Attia, G. Balasundaram, M. Moothanchery, U. Dinish, R. Bi, V. Ntziachristos, M. Olivo, A review of clinical photoacoustic imaging: Current and future trends, Photoacoustics 16 (2019) 100144.
[29] W. Qiu, J.H. Joergensen, E. Corato, H. Bruus, P. Augustsson, Fast microscale acoustic streaming driven by a temperature-gradient-induced nondissipative acoustic body force, Phys. Rev. Lett. 127 (2021) 064501.
[30] C.-I. Lin, M. Baker, R.J. Charlson, Absorption coefficient of atmospheric aerosol: A method for measurement, Appl. Opt. 12 (6) (1973) 1356–1363.
[31] R. Siegel, J. Howell, Thermal radiation heat transfer, 1972.
[32] A. Offner, R. Yang, D. Felman, N. Elkayam, Y. Agnon, G.Z. Ramon, Acoustic oscillations driven by boundary mass exchange, J. Fluid Mech. 866 (2019) 316–349.
[33] R. Yang, N. Blanc, A. Vardi-Chouchana, N. Ouzana, G.Z. Ramon, PC-TAS: A design environment for phase-change and classical thermoacoustic systems, SoftwareX 19 (2022) 101142.
[34] R. Yang, A. Meir, G. Ramon, Theoretical performance characteristics of a travelling-wave phase-change thermoacoustic engine for low-grade heat recovery, Appl. Energy 261 (2020) 114377.
[35] X. Zhang, J. Chang, Onset and steady-operation features of low temperature differential multi-stage travelling wave thermoacoustic engines for low grade energy utilization, Energy Convers. Manage. 105 (2015) 810–816.
[36] T. Jin, R. Yang, Y. Wang, Y. Feng, K. Tang, Low temperature difference thermoacoustic prime mover with asymmetric multi-stage loop configuration, Sci. Rep. 7 (1) (2017) 7665.
[37] Z. Wu, L. Zhang, W. Dai, E. Luo, Investigation on a 1kW traveling-wave thermoacoustic electrical generator, Appl. Energy 124 (2014) 140–147.